



OPEN Compact way to generate guide star for wavefront sensing in Bessel two-photon microscopy

Fanglin Luo^{1,3,4}, Nan Li^{1,3,4}, Chengliang Yang^{1,3}, Zenghui Peng^{1,3}, Quanquan Mu^{1,3} & Xingyun Zhang^{2,3}✉

We introduce a compact method for generating guide stars to enable direct wavefront sensing in Bessel two-photon microscopy. By sequentially modulating an axicon phase and a thin lens phase using a spatial light modulator (SLM), our approach achieves seamless switching between Bessel and Gaussian illumination beams without requiring mechanical movement or additional optical components. The Bessel beam provides an expanded field of view for imaging, while the Gaussian beam serves as a point-like guide star for wavefront sensing. Experimental validation in a Bessel two-photon light sheet microscope demonstrates that wavefront correction based on our method enhances the signal-to-noise ratio (SNR) by 7.3 times and improves axial resolution by 4.4 times.

Bessel beams maintain their shape and size over long distances, even when encountering obstacles or diffraction effects, owing to their non-diffracting nature¹. When combined with two-photon excitation using a near-infrared femtosecond laser, they enable a narrow focus with an extended depth of field². Consequently, two-photon microscopy with Bessel illumination beam has been widely adopted for biological imaging, including studies of neuronal networks, cellular dynamics, and tissue morphology. It excels in imaging thick samples—such as brain slices or intact organs—where conventional microscopy struggles due to light scattering and limited penetration depth^{3–6}.

Biological tissue is a complex, heterogeneous medium with spatially varying refractive indices. As illumination light propagates through tissue, refractive index inhomogeneities induce wavefront aberrations, distorting the light path. These aberrations cause significant dispersion and attenuation of light intensity, worsening with penetration depth. Ultimately, they impair two-photon excitation efficiency, degrading both the illumination field of view and fluorescence image quality⁷.

Adaptive optics (AO), initially developed to compensate for atmospheric turbulence in astronomical telescopes^{8,9}, is the most effective method for mitigating wavefront aberrations in optical systems. AO employs a wavefront sensor to detect distortions and a corrector (e.g., deformable mirror) to compensate for them. Accurate wavefront sensing is thus pivotal for AO implementation, posing a key challenge in fluorescence microscopy.

Two primary approaches exist for detecting tissue-induced aberrations: (1) Indirect Sensing^{10–12}. This sensorless method iteratively optimizes the wavefront corrector based on fluorescence intensity feedback. While simple, it is limited to low-order aberrations and suffers from slow convergence. (2) Direct Sensing^{13–15}. A fluorescent “guide star” (a point-like emitter) is generated within the sample, and its emitted light is analyzed by a wavefront sensor. This method enables high-speed, high-precision detection of high-order aberrations, making it more suitable for practical applications.

In two-photon microscopy with Gaussian illumination, direct wavefront sensing is straightforward because the Gaussian focus itself acts as a guide star. However, under Bessel-beam illumination, two-photon fluorescence produces an elongated “line target” along the optical axis, which cannot serve as a guide star. Current workarounds include introducing an auxiliary Gaussian beam (as in lattice light-sheet microscopy¹⁶ or modifying the optical setup to generate a Gaussian beam by adjusting optical components¹⁷). While feasible, these approaches complicate system design and alignment. Developing a streamlined method for direct aberration sensing in Bessel two-photon microscopy remains an open challenge. Overcoming this hurdle could lower the application barriers of adaptive optics in Bessel two-photon microscopy, thereby providing convenience for the system optical design.

¹State Key Laboratory of Advanced Manufacturing for Optical Systems, Chinese Academy of Sciences, Changchun 130033, China. ²Beam Precision Control Research Laboratory, Changchun Institute of Optics, Fine Mechanics and Physics, Chinese Academy of Sciences, Changchun 130033, China. ³Center of Materials Science and Optoelectronics Engineering, University of Chinese Academy of Sciences, Beijing 100049, China. ⁴Fanglin Luo and Nan Li contributed equally to this work ✉email: xyzhang@ciomp.ac.cn

Methods

We present a compact method for generating guide stars to enable direct wavefront sensing in Bessel two-photon microscopy. Our approach utilizes a spatial light modulator (SLM) to generate Bessel beams and facilitate switching between Bessel and Gaussian beam modes. Figure 1 illustrates the working principle of the method, where we have simplified the schematic by omitting the 4f lens system (for beam expansion and aperture conjugation) and scanning devices. For clarity, the SLM is depicted as a transmissive element, though in practice it operates reflectively. The key innovation lies in positioning the SLM at a fixed displacement distance s from the back focal plane of lens L. This specific configuration enables the crucial switching mechanism between Bessel and Gaussian beam modes.

As illustrated in Fig. 1a, the incident near-infrared femtosecond laser is modulated by the SLM with an axicon phase profile Φ_B to generate a Bessel beam. The lens L and objective lens IO form a 4f imaging system, ensuring the illumination beam maintains its Bessel profile in the sample plane. The SLM is positioned at a distance of $s+f$ (rather than f , the focal length of lens L) from lens L. This configuration causes only a slight displacement of the Bessel beam from IO's focal plane while preserving its characteristic intensity profile. As shown in Eq. (1), the axicon phase Φ_B is described by concentric rings in the SLM's pixel coordinates (x, y) , where the ring width parameter r_0 (where the phase changes from 0 to 2π) determines both the transverse width and propagation length of the resulting Bessel beam. And $\text{mod}(a, b)$ denotes the modulo operation of a by b .

$$\Phi_B(x, y) = \text{mod} \left(2\pi \sqrt{x^2 + y^2} / r_0, 2\pi \right) \quad (1)$$

For wavefront sensing, the SLM phase pattern switches to a thin lens profile Φ_L , as shown in Eq. (2) (where $k = 2\pi/\lambda$, and λ represents the wavelength of the laser). In this mode, the SLM effectively becomes a lens with focal length s , forming a 4f system with lens L. This produces a Gaussian beam at the objective's entrance pupil, which IO focuses to create a point-like guide star in the sample, as shown in Fig. 1b. The two-photon fluorescence from this guide star is collected by IO, reflected by the dichroic mirror (DM), and directed to the wavefront sensor (WFS). Due to the two-photon excitation process, the fluorescence wavelength (slightly $> \lambda/2$) differs sufficiently from the illumination laser wavelength for effective spectral separation by the DM.

$$\Phi_L(x, y) = \text{mod} \left(-\frac{k}{2s}(x^2 + y^2), 2\pi \right) \quad (2)$$

This approach enables seamless switching between Bessel and Gaussian illumination modes using only phase modulation from the SLM, eliminating the need for mechanical movement or additional optical components.

Results

To verify the proposed method, we set up an experimental apparatus (Bessel two-photon light sheet microscopy) as shown in Fig. 2. The whole setup can be divided into three optical paths. (1) Illumination path: femtosecond laser is expanded by beam expander (BE), then reflected by a spatial light modulator (SLM) with small angle (less than 10°). SLM is modulated with axicon phase Φ_B or thin lens phase Φ_L to generate Bessel beam or Gauss focus. Then transmitted with two 4F systems (L1–L2 and L3–IO) to form Bessel illumination or Gauss guide star in the sample. (2) Imaging path: The two-photon fluorescence excited by illumination light is collected by the detection objective DO (perpendicular to IO), and captured by Camera passing through Filter and lens L4. (3) Aberration sensing path: The two-photon fluorescence of guide star is collected by IO and propagates backward along the illumination path. After being de-scanned by galvo scanner (GS), it is reflected by the dichroic mirror (DM) and ultimately enters the wavefront sensor (WFS) for aberration detection. Note: Mirror M3 and GS effectively form a “climbing frame” in the Y-direction. This design enables GS to scan around the Z-axis, allowing the Bessel illumination beam along the X-direction to create a light sheet illumination in the XY plane of the sample. Figure 2b shows a top view photo of the experimental setup along the Y-direction, M3 is physically obscured by GS and is not labeled in the photo.

The details of the optical devices are as follows: The illumination laser is a femtosecond laser with 920 nm wavelength, 100 fs pulse width and 80 MHz repetition rate. SLM is a Meadowlark liquid crystal spatial light modulator with 12.8 mm aperture and 512×512 pixels. The focal lengths of lens L1 ~ L6 are 200 mm, 80 mm, 180 mm, 200 mm, 200 mm and 300 mm respectively. DM transmits light bands above 700 nm and reflects light

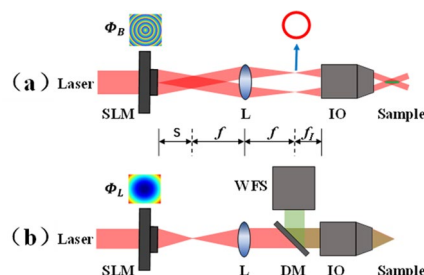


Fig. 1. Principle of switching between Bessel beam and Gauss beam.

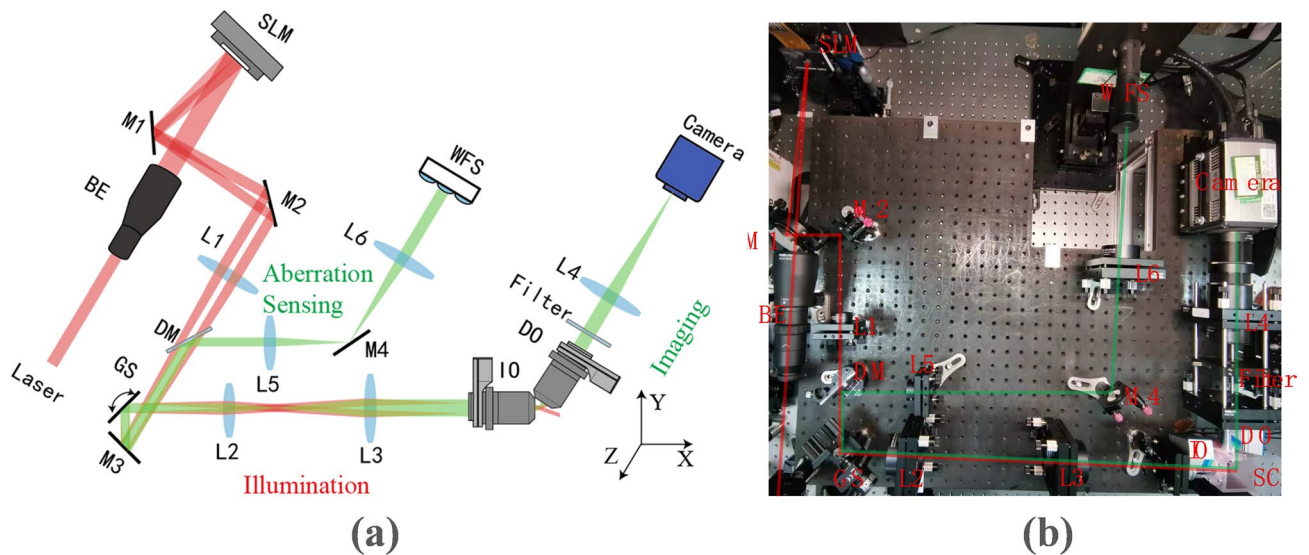


Fig. 2. (a) Optical layout and (b) photon of Experimental apparatus.

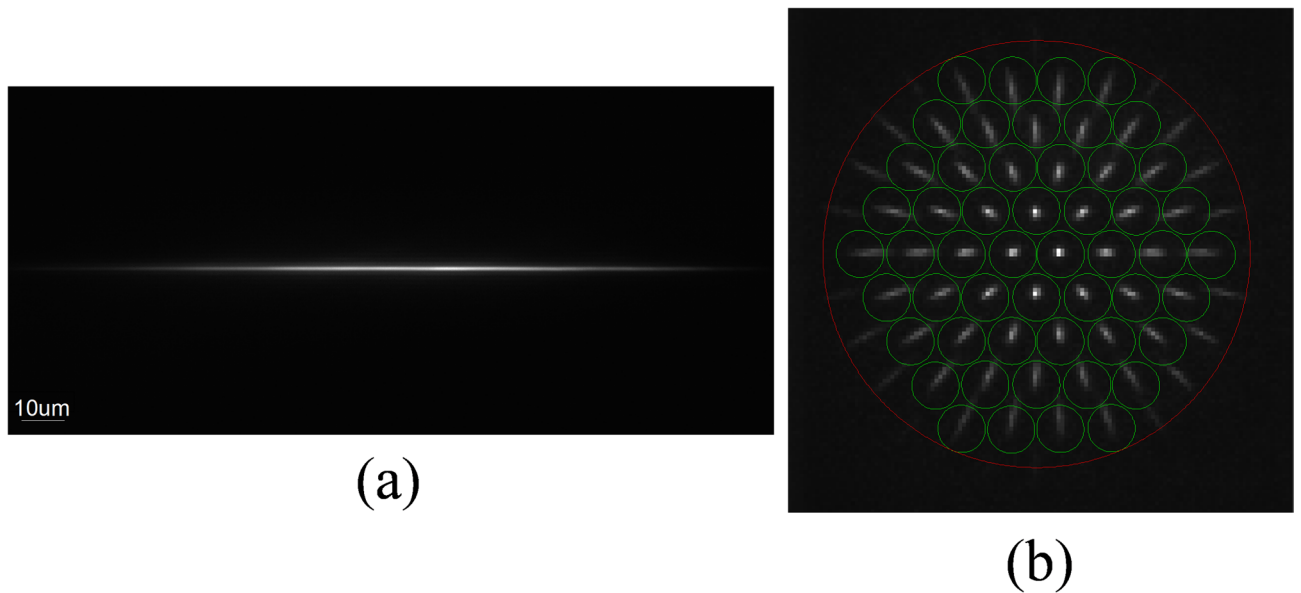


Fig. 3. The Bessel fluorescence captured by the Camera (a) and WFS (b). Scale bar: 10 μm .

bands below 700 nm. GS (GVS011, Thorlabs) has a maximum scan angle of $\pm 20^\circ$. The focal lengths of IO and DO are both 5 mm, and numerical aperture both 0.8. The cutoff wavelength of the short-pass Filter (FESH0700, Thorlabs) is 700 nm. Camera is an Andor sCMOS with 2048×2048 pixels and $6.5 \mu\text{m}$ pixel size. WFS is a custom Shark-Hartmann wavefront sensor with 6.1 mm aperture. SC is a custom sample chamber. The distance between SLM and L1, L1 and GS, GS and L2, L2 and L3, L3 and IO, DO and L4, GS and L5, L5 and L6, L6 and WFS are 500 mm, 200 mm, 80 mm, 260 mm, 185 mm, 205 mm, 200 mm, 500 mm, 300 mm, respectively.

Our design eliminates the conventional annular mask typically required to block non-diffracted light in SLM-generated Bessel beams¹⁷. Experimental results demonstrate that when using a high-efficiency ($> 90\%$) dielectric mirror-coated SLM, non-diffracted light has negligible impact on two-photon excitation.

With this optical configuration, when the SLM modulates the axicon phase Φ_B (Eq. (1), parameter $r_0 = 200 \mu\text{m}$), the illumination forms a Bessel beam in the sample. Using Rhodamine 6G solution for evaluation, the excited two-photon fluorescence captured by the camera shows a beam thickness of $0.89 \mu\text{m}$ and length of $94.25 \mu\text{m}$, as shown in Fig. 3a. The WFS-captured fluorescence reveals non-point-like spots elongated in different directions (minimal near the optical axis, increasing with off-axis distance), as shown in Fig. 3b. This occurs because the fluorescence originates from an axial line source rather than a point source. The severe elongation of peripheral spots (extending beyond microlens boundaries) and their low SNR make the WFS

inoperable. This aberration-free scenario (using homogeneous refractive index solution) demonstrates that even ideal Bessel beams cannot serve as WFS guide stars - particularly problematic for biological samples.

When the SLM instead modulates the thin lens phase Φ_L (Eq. (2), parameter $s=300$ mm), it effectively becomes a 300 mm lens. Combined with L1 (200 mm focal length, 500 mm spacing), they form a 4f system that delivers Gaussian illumination to the objective. The resulting two-photon fluorescence measures 0.87 μm thick and 3.9 μm long, as shown in Fig. 4a. The WFS spots appear as uniform spots suitable for wavefront sensing, as shown in Fig. 4b. The measured wavefront (PV = 0.24 λ , RMS = 0.03 λ < $\lambda/30$) confirms both the Gaussian beam's suitability as a guide star and the apparatus's negligible system aberrations, as shown in Fig. 4c.

To evaluate our method's performance, we inserted an astigmatic film (commercially obtained astigmatic correction lens specifically designed for professional ophthalmic testing) at IO's rear pupil (between L3 and IO in Fig. 2). With Φ_L modulation, the WFS-measured Zernike coefficients (Noll's sequence) show dominant astigmatism (modes 4–5) with other modes below the 1/14 λ measurement error, as shown in Fig. 5a. The reconstructed wavefront shows PV = 4.36 λ and RMS = 0.74 λ , as shown in Fig. 5b. We also independently measured the aberration of this lens using a ZYGO interferometer and confirmed that it contains almost only astigmatic aberration.

Further validation used 100 nm fluorescent beads (Invitrogen, F8803) in 1.5% agarose, imaged under three conditions: (a) no aberration, (b) with aberration (no correction), (c) with aberration and AO correction, as shown in Fig. 6. 3D projection videos in three scenarios can more intuitively demonstrate the effect of AO

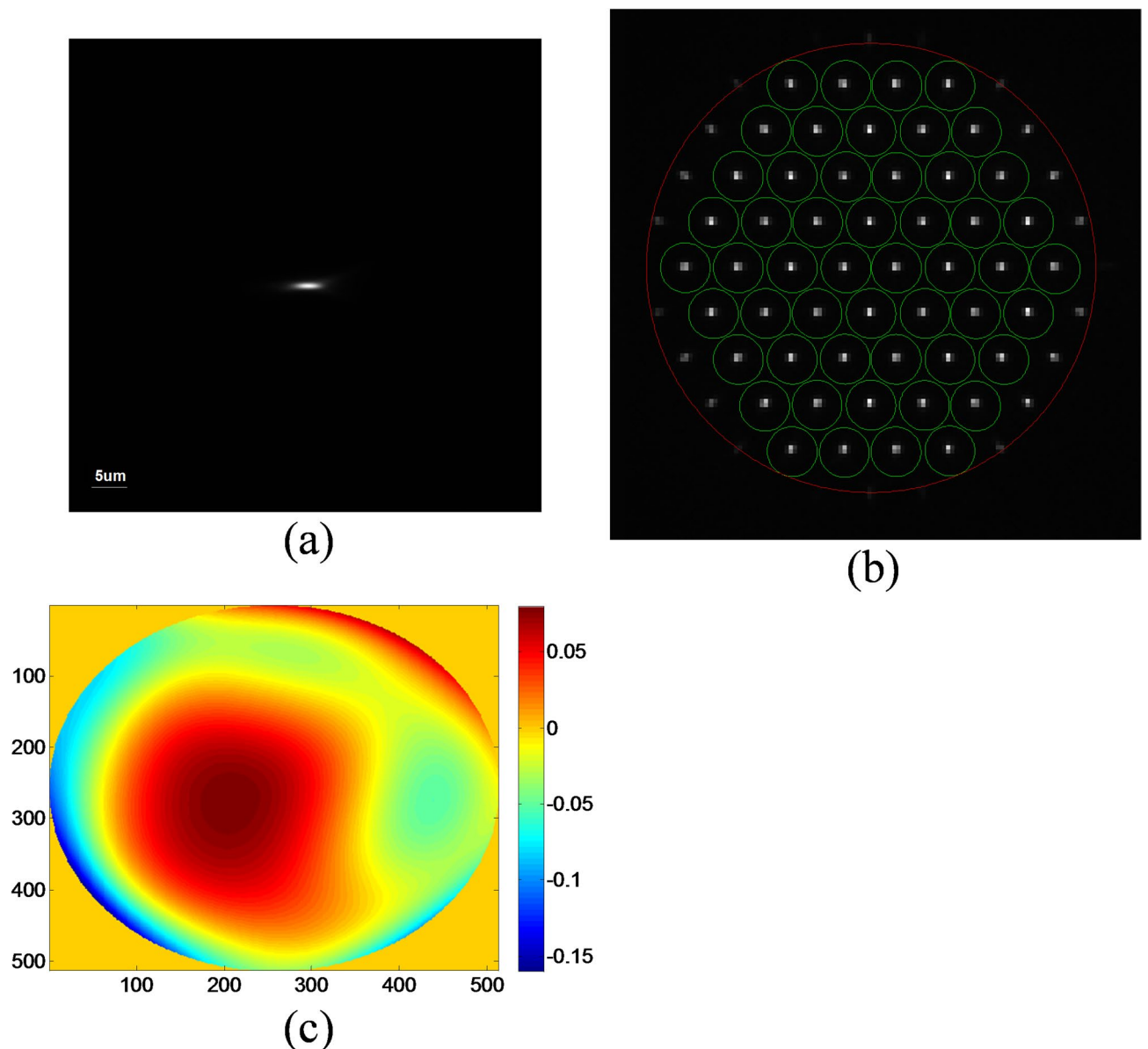


Fig. 4. The Gauss fluorescence captured by the Camera (a) and WFS (b). (c) Measured wavefront. Scale bar in (a): 5 μm . Color bar in (c): $-0.15 \sim 0.05 \lambda$.

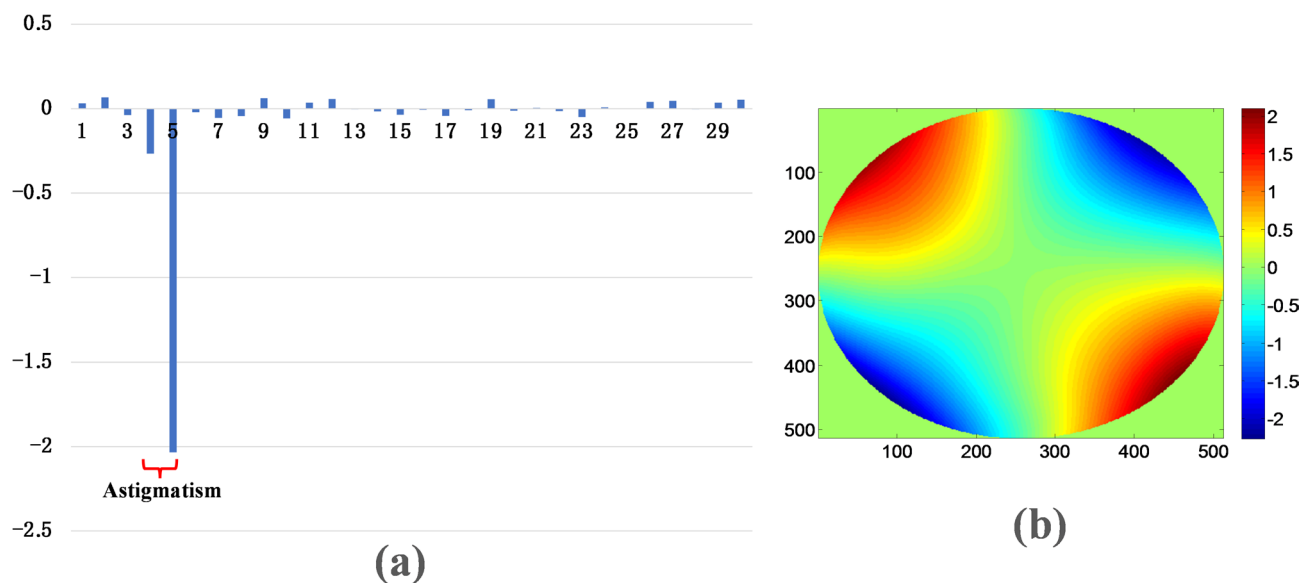


Fig. 5. The phase of the astigmatic film detected with Gauss beam: **(a)** Zernike coefficients; **(b)** Wavefront.

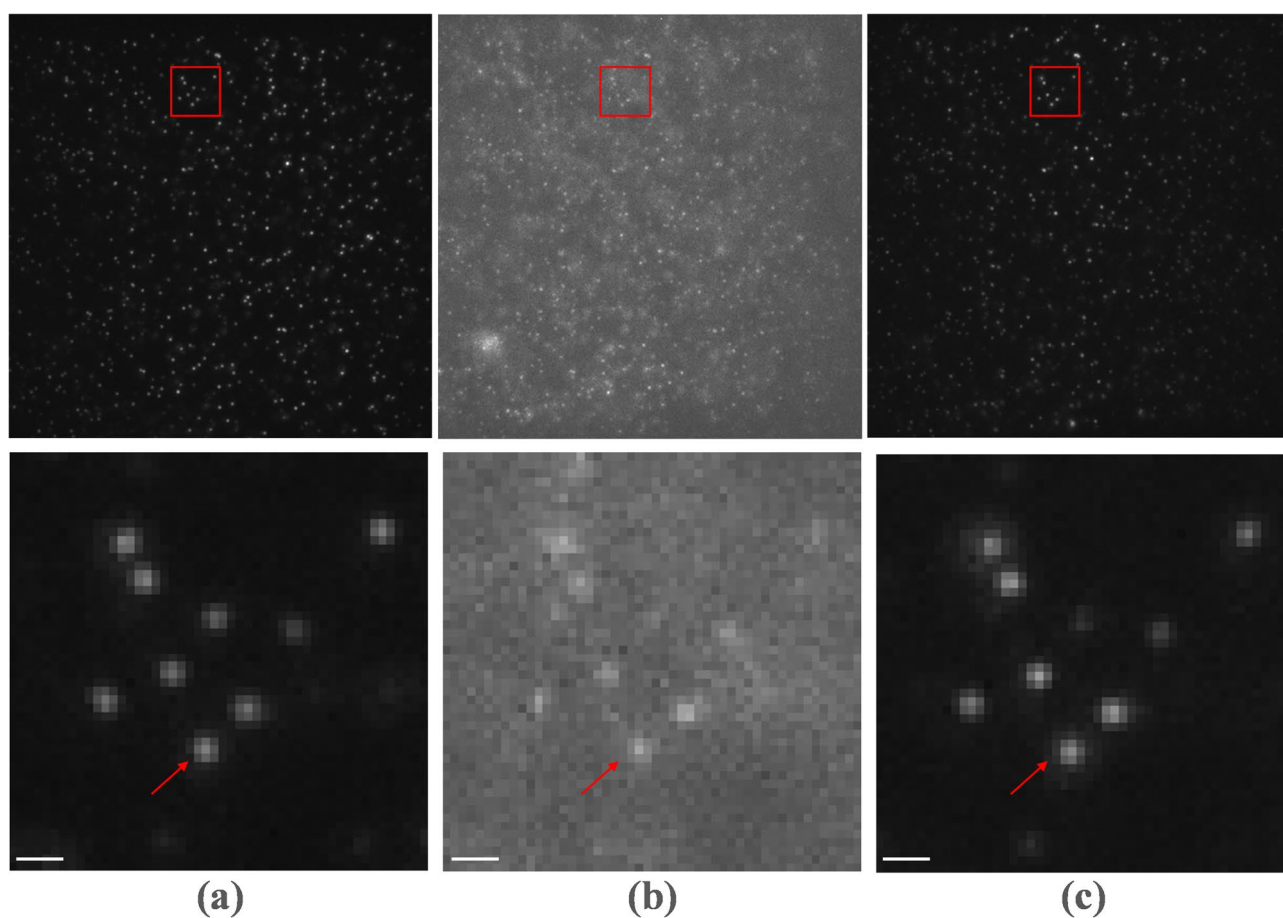


Fig. 6. Images of fluorescent beads under the same exposure time: **(a)** without aberration; **(b)** with aberration and no AO; **(c)** with aberration and AO. The images in the bottom row are zoomed-in views of the red-boxed region in the top row. Scale bars: 1.0 μm .

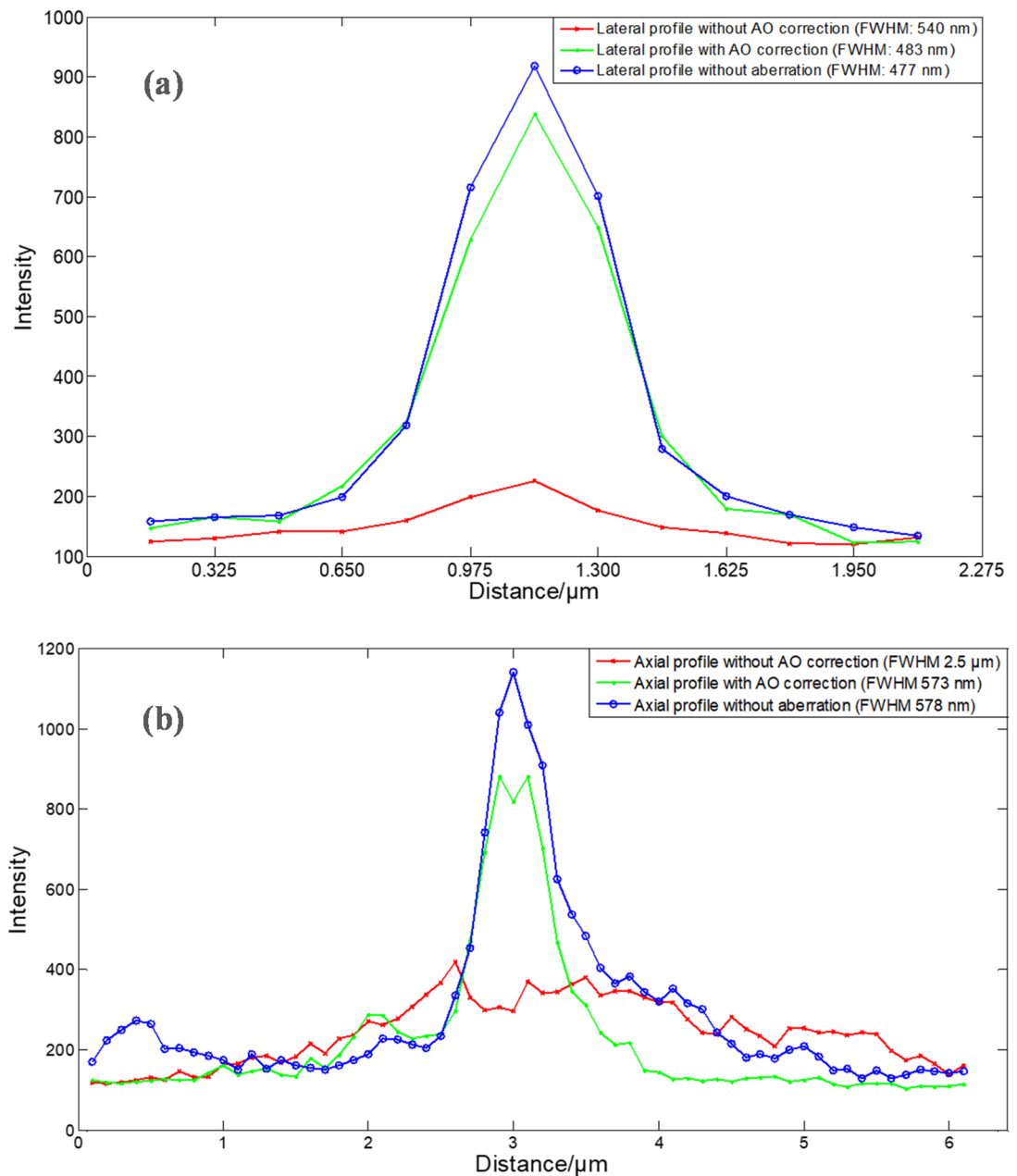


Fig. 7. Profiles of the fluorescent bead identified by red arrows in Fig. 6: (a) Lateral; (b) Axial.

correction, visible in supplementary video 1–3. AO correction is done by our wavefront sensing method and focal correction method¹⁶ (see more details in Supplementary Fig. S1).

As shown in Fig. 7a, lateral profiles of the arrow-marked bead show similar FWHM values (477 nm, 540 nm, 483 nm respectively, at 162.5 nm/pixel magnification). While aberration in illumination path minimally affects lateral resolution of light sheet microscopies, AO improves SNR by 7.3 \times by reducing illumination dispersion and intensity loss. Axial sectioning (0.1 μm steps) reveals aberration in illumination path has greater impact on axial resolution, as shown in Fig. 7b: FWHM values of 578 nm (no aberration), 2.5 μm (uncorrected), and 573 nm (corrected). The 4.4 \times resolution improvement after AO demonstrates our method's accuracy in detecting and compensating illumination-path aberrations.

In summary, we present a straightforward yet effective method for generating guide stars to enable direct wavefront sensing in Bessel two-photon microscopy, establishing the foundation for implementing adaptive optics to compensate for sample-induced aberrations in such systems. Although our validation experiments were conducted specifically in the illumination path of a Bessel two-photon light sheet microscope, the proposed guide star generation method can equally be applied to measure aberrations in the detection path. Furthermore, this approach is readily adaptable to other microscopes using SLM-modulated Bessel beam illumination and is not limited to two-photon applications.

Data availability

Data supporting the findings of this study are available from the corresponding author on reasonable request, subject to data transfer agreement.

Received: 30 April 2025; Accepted: 13 October 2025

Published online: 18 November 2025

References

1. Durnin, J., Miceli, J. J. & Eberly, J. H. Diffraction free beams. *Phys. Rev. Lett.* **58**, 15 (1987).
2. Botcherby, E. J., Juškaitis, R. & Wilson, T. Scanning two photon fluorescence microscopy with extended depth of field. *Opt. Commun.* **268** (2), 253–260 (2006).
3. Takanezawa, S., Saitou, T. & Imamura, T. Wide field light-sheet microscopy with lens-axicon controlled two-photon Bessel beam illumination. *Nat. Commun.* **12**, 2979 (2021).
4. Li, S. et al. Self-reconstructing Bessel beam created by two-photon-polymerized micro-axicon for light-sheet fluorescence microscopy. *Results Phys.* **24**, 104111 (2021).
5. Fan, J. L. et al. High-speed volumetric two-photon fluorescence imaging of neurovascular dynamics. *Nat. Commun.* **11** (1), 6020 (2020).
6. He, H. et al. Resolution enhancement in extended depth of field for volumetric two-photon microscopy. *Opt. Lett.* **45** (11), 3054–3057 (2020).
7. Schwertner, M., Booth, M. J. & Wilson, T. Characterizing specimen induced aberrations for high NA adaptive optical microscopy. *Opt. Express.* **12** (26), 6540–6552 (2004).
8. Booth, M. J. Adaptive optics in microscopy. *Philos. Trans. R Soc. Lond. A.* **365** (1861), 2829–2843 (2007).
9. Zhang, X. et al. Progress of liquid crystal adaptive optics for applications in ground-based telescopes. *Mon. Not. R. Astron. Soc.* **494**, 3536 (2020).
10. Débarre, D. et al. Image-based adaptive optics for two-photon microscopy. *Opt. Lett.* **34** (16), 2495–2497 (2009).
11. Tang, J., Germain, R. N. & Cui, M. Superpenetration optical microscopy by iterative multiphoton adaptive compensation technique. *Proc. Natl. Acad. Sci.* **109** (22), 8434–8439 (2012).
12. Kim, H. et al. Modal focal adaptive optics for Bessel-focus two-photon fluorescence microscopy. *Opt. Express.* **33** (1), 680–693 (2025).
13. Wang, K. et al. Direct wavefront sensing for high-resolution in vivo imaging in scattering tissue. *Nat. Commun.* **6** (1), 7276 (2015).
14. Wilding, D., Pozzi, P., Soloviev, O., Vdovin, G. & Verhaegen, M. Adaptive illumination based on direct wavefront sensing in a light-sheet fluorescence microscope. *Opt. Express.* **24** (22), 24896–24906 (2016).
15. Zheng, W. et al. Adaptive optics improves multiphoton super-resolution imaging. *Nat. Methods.* **14** (9), 869–872 (2017).
16. Liu, T. L. et al. Observing the cell in its native state: imaging subcellular dynamics in multicellular organisms. *Science* **360**, 6386 (2018).
17. Chen, W. et al. In vivo volumetric imaging of calcium and glutamate activity at synapses with high spatiotemporal resolution. *Nat. Commun.* **12** (1), 6630 (2021).

Acknowledgements

The author thanks the CAS Interdisciplinary Innovation Team for support for this work.

Author contributions

F.L. and N.L. are joint first authors and contributed equally. F.L.: data collection, data analysis, co-wrote the manuscript. N.L.: optical design, data analysis, co-wrote the manuscript. C.Y., Z.P. and Q.M.: study design, reviewed and edited the manuscript. X.Z.: designed and conceived the study, obtained funding, co-wrote the manuscript.

Funding

National Natural Science Foundation of China (62475258).

Declarations

Competing interests

The authors declare no competing interests.

Additional information

Supplementary Information The online version contains supplementary material available at <https://doi.org/10.1038/s41598-025-24341-9>.

Correspondence and requests for materials should be addressed to X.Z.

Reprints and permissions information is available at www.nature.com/reprints.

Publisher's note Springer Nature remains neutral with regard to jurisdictional claims in published maps and institutional affiliations.

Open Access This article is licensed under a Creative Commons Attribution-NonCommercial-NoDerivatives 4.0 International License, which permits any non-commercial use, sharing, distribution and reproduction in any medium or format, as long as you give appropriate credit to the original author(s) and the source, provide a link to the Creative Commons licence, and indicate if you modified the licensed material. You do not have permission under this licence to share adapted material derived from this article or parts of it. The images or other third party material in this article are included in the article's Creative Commons licence, unless indicated otherwise in a credit line to the material. If material is not included in the article's Creative Commons licence and your intended use is not permitted by statutory regulation or exceeds the permitted use, you will need to obtain permission directly from the copyright holder. To view a copy of this licence, visit <http://creativecommons.org/licenses/by-nc-nd/4.0/>.

© The Author(s) 2025